A high abundance of massive galaxies 3–6 billion years after the Big Bang

Karl Glazebrook[1], **Roberto G. Abraham**[2], **Patrick J. McCarthy**[3], **Sandra Savaglio**[1], **Hsiao-Wen Chen**[4], **David Crampton**[5], **Rick Murowinski**[5], **Inger Jørgensen**[6], **Kathy Roth**[6], **Isobel Hook**[7], **Ronald O. Marzke**[8] **& R. G. Carlberg**[2]

[1] *Department of Physics & Astronomy, Johns Hopkins University, 3400 North Charles Street, Baltimore, Maryland 21218-2686, USA*
[2] *Department of Astronomy & Astrophysics, University of Toronto, 60 St George Street, Toronto, Ontario M5S 3H8, Canada*
[3] *Observatories of the Carnegie Institute of Washington, Santa Barbara Street, Pasadena, California 9110, USA*
[4] *Center for Space Research, Massachusetts Institute of Technology, Cambridge, Massachusetts 02139-4307, USA*
[5] *Herzberg Institute of Astrophysics, National Research Council, 5071 West Saanich Road, Victoria, British Columbia, V9E 2E7, Canada*
[6] *Gemini Observatory, Hilo, Hawaii 96720, USA*
[7] *Department of Astrophysics, Nuclear & Astrophysics Laboratory, Oxford University, Keble Road, Oxford OX1 3RH, UK*
[8] *Department of Physics and Astronomy, San Francisco State University, 1600 Holloway Avenue, San Francisco, California 94132, USA*

Hierarchical galaxy formation is the model whereby massive galaxies form from an assembly of smaller units[1]. The most massive objects therefore form last. The model succeeds in describing the clustering of galaxies[2], but the evolutionary history of massive galaxies, as revealed by their visible stars and gas, is not accurately predicted. Near-infrared observations (which allow us to measure the stellar masses of high-redshift galaxies[3]) and deep multi-colour images indicate that a large fraction of the stars in massive galaxies form in the first 5 Gyr (refs 4–7), but uncertainties remain owing to the lack of spectra to confirm the redshifts (which are estimated from the colours) and the role of obscuration by dust. Here we report the results of a spectroscopic redshift survey that probes the most massive and quiescent galaxies back to an era only 3 Gyr after the Big Bang. We find that at least two-thirds of massive galaxies have appeared since this era, but also that a significant fraction of them are already in place in the early Universe.

Star-formation rates in the high-redshift ($z > 1$) Universe have been probed by measuring rest-frame ultraviolet (UV) emission[8] of galaxies. The UV is dominated by newly formed massive stars but can be highly obscured[9]. Moreover, star-formation in galaxies is a stochastic phenomenon and correlates poorly with mass: the most massive galaxies in the local Universe are giant ellipticals and they have very weak UV emission[10], which makes them difficult to detect at $z > 1$. Direct determination of dynamical masses of galaxies requires spatially resolved velocity measurements of galaxies—this has been done out to $z \approx 1$ (refs 11,12), but such observations are very challenging at higher redshifts owing to signal-to-noise limitations.

An alternative approach is to infer the total mass in stars from red light, which traces accumulated stellar populations. Studies[3] have shown that stellar mass correlates extremely well with dynamical mass out to $z = 1$. Stellar mass evolution can be predicted by using galaxy formation models based on cosmological numerical simulations augmented with analytical star-formation recipes[13], which adopt simplified prescriptions for various heating and cooling processes in the interstellar medium[13,14].

Deep near-infrared data provide a window on stellar masses of galaxies at high redshift. This light is dominated by the old, evolved stellar populations in galaxies, and is little affected by transient star-formation[15] or dust obscuration. To a good approximation, the total K-band light traces the accumulation of stellar mass; equivalently, one can say that the stellar mass-to-light ratio ($M/L_{\rm K}$) is nearly constant, with little dependence on the previous star-formation history (SFH). In fact, rest-frame $M/L_{\rm K}$ varies only by a factor of two between extremely young and extremely old galaxy stellar populations: in contrast, $M/L_{\rm B}$ can vary by more than a factor of ten[16], and $M/L_{\rm UV}$ varies tremendously (reaching as low as 1% of the solar value) because the UV light is dominated by the instantaneous star-formation rate (SFR) rather than the stellar mass. Even at redshifts up to $z = 2$, the observed-frame K-band probes the rest-frame R-band which is still dominated by old stellar populations. The $M/L_{\rm R}$ variation is still less than a factor of four, partly due to the youth of the Universe at that redshift.

We use the Gemini Deep Deep Survey (GDDS)[17] to define a new sample of 150 galaxies with $K < 20.6$ mag and $0.8 < z < 2$ located in four independent 30 arcmin^2 fields. The spectroscopic identification completeness is 89%. The determination of stellar masses for each galaxy follows standard multi-color stellar population fitting techniques; this approach is fairly general and robust, and is detailed in Methods. We find that the K-band light traces the stellar mass quite well: evolutionary changes in galaxy numbers with redshift are much more important than changes in colour. The findings presented below are simply driven by the presence of numerous $K \approx 20$ galaxies at $z > 1.5$, which must be massive objects.

Figures 1 and 2 illustrate the nature of the most massive galaxies. They are found by the GDDS to $z = 2$ at $K \approx 20$, even when they are very red ($I - K > 4$). The red galaxies are predominantly red owing to old stellar populations (these are GDDS spectral classes[17] '001' and '011', showing photospheric features from evolved stars) and not dust reddening of young lower-mass galaxies. The red, old

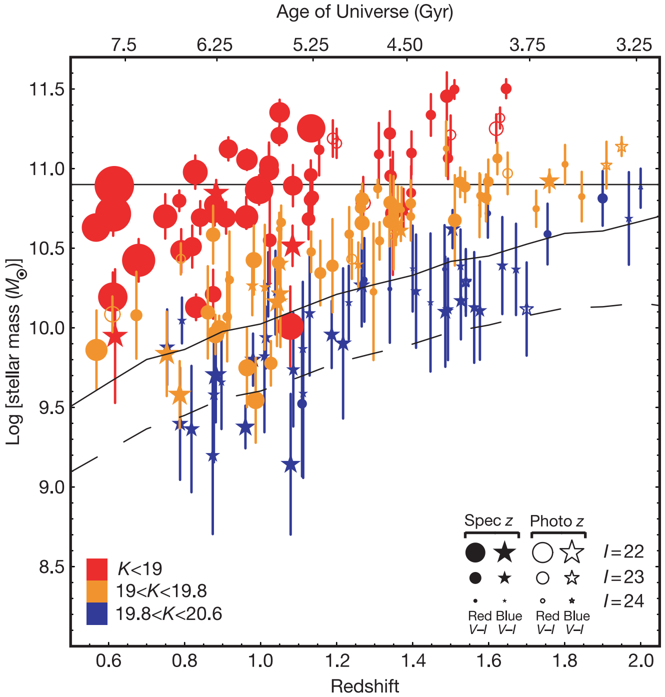

Figure 1 Stellar mass–redshift distribution for our galaxies. The 1σ error bars come from the Monte Carlo mass fitting. Symbol colours code the observed K-band magnitude (see key on left). Solid/open symbol shapes denote spectroscopic/photometric redshifts respectively. Circle/star symbols denote objects respectively redder/bluer in $V - I$ than a model Sbc galaxy template[30]. Symbol size is keyed to the I-band magnitude. The horizontal line denotes the characteristic Schechter mass scale in the local Universe[20]. The solid curve shows how the K-band flux limit translates into a mass completeness limit for a maximally old simple stellar population (SSP). The dashed curve shows an example mass limit for bluer objects (SFR = const. model).

galaxies make a large contribution (30%) to the stellar mass in the Universe in the redshift range $1.2 < z < 1.8$. Also at $z > 1$ there are a number of blue galaxies despite this being a K-selected sample. These correspond to massive star-forming galaxies which have high metal abundances[18].

The cumulative stellar mass density per unit volume in each redshift bin down to various mass thresholds (Fig. 3; Table 1) is computed following the standard maximum volume $V/V_{\max}$ formalism (this corrects for the smaller redshift ranges covered by fainter objects[19]) for a $K < 20.6$ limit and weighting by the sampling. We use K-corrections from our individual spectral energy distribution (SED) fits, but the results do not depend strongly on the details of the K-correction. Although a K-selected sample is a good proxy for a mass-selected sample, it is still necessary to consider incompleteness as a function of M/L. To do this, we compute the maximum possible M/L at each redshift for a model galaxy as old as the Universe which formed all its stars at once (a 'simple stellar population', or SSP). This M/L is converted to a mass limit (via the K-band flux limit and the K-correction) and is shown in Fig. 1. We are complete above this mass limit; bluer objects can be seen below this limit. Bins that might miss high M/L objects are plotted as lower limits in Fig. 3. The error bars are calculated from shot noise on the number of galaxies in each bin. These do not include the effects of large-scale structure, but we believe these are not significant because our GDDS fields are large, were selected from even larger-area images in regions near average density[17] (that is, neither highly over-dense nor under-dense) and because our colour-dependent weights normalize to the full imaging area (554.7 arcmin^2) which would counteract the additional clustering of red objects. Finally, we have performed the check of splitting the sample by different fields (different independent sight-lines). The same general results are found for these, albeit with larger errors. We have also assessed the effect of the mass fitting errors on the mass densities with our Monte Carlo methods; this is not a significant source of error. In every bin, galaxies with spectroscopic redshifts dominate the mass budget, except for the $1.6 < z < 2$ and $M > 10^{10.8} M_\odot$ bin, where the spectroscopic completeness is only 50% and we augment our spectroscopy with photometric redshifts. Analysing the sub-sample with only spectroscopic redshifts results in no significant changes to any bin except for this one (which is thus 0.3 dex lower); the essential scientific result is unchanged.

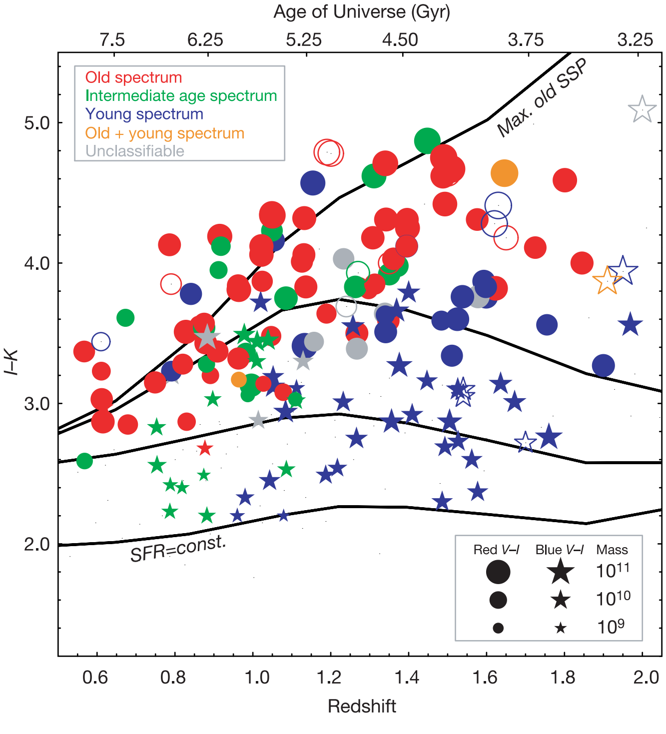

Figure 2 Colour–redshift distribution for our galaxies. Observed frame $I - K$ colour is plotted with symbol size keyed to mass, shape to optical $V - I$ colour (as in Fig. 1) and symbol colour keyed to the spectral classification (see key at top). Solid/open symbols denote spectroscopic/photometric redshifts. Model tracks (solid lines) are shown ranging from a maximally old SSP through to SFR = const., for synthetic solar metallicity galaxies which form at $z = 10$. (Note the points red-ward of the old track at $z = 0.6$ may be artificially reddened by observational aperture/metallicity effects; this is insignificant for $z > 0.8$.)

There is a clear decline with redshift in stellar mass locked up in the most massive galaxies. This trend is in accord with ideas of gradual assembly. However, it declines only slowly towards high redshift and, surprisingly, the massive galaxies do not decline more rapidly than the whole population. We note that galaxies with $M > 10^{10.8} M_\odot$ are brighter than our flux limits (for any possible M/L value) throughout our redshift range; a regression on these gives an acceptable fit for $\rho \propto (1 + z)^{-1.7 \pm 1.6}$. At $z = 1$ the mass densities for the $M > 10^{10.8} M_\odot$ sample are 38 (±18)% of their local value[20]; at $z = 1.8$ this becomes 16 (±6)%. These results for the most massive galaxies are consistent with previous Hubble Deep Field South photometric redshift determinations[4,5], but inconsistent with the more rapid decline (a factor of ~ 6 over $0 < z < 1$) found with photometric redshifts by the Munich Near-Infrared Cluster Survey[6] (however we note that their SED fitting forces maximally old galaxies at all redshifts, which could be problematic). Overlaid on Fig. 3 (shaded region) is the range of estimates for the growth of total stellar mass based on the integral of the observed rest-UV derived SFR–z relationship. (These are based on the analytic fit[20] of points from Fig. 9 of ref. 9, both with and without extinction correction, integrated using PEGASE.2[21].) Our uppermost points represent lower limits on the total stellar mass density, and we confirm previous findings that an extinction correction is essential for UV SFR estimates to be consistent with stellar mass measurements[4,20].

Theoretical models of galaxy formation convert gas into stars in dark matter haloes using semi-empirical recipes, and must satisfy three key observables: the first is the distribution of local galaxy luminosities, the second is the distribution of galaxy colours and the third is the abundance of massive galaxies at high redshift. The last of these has until now been the most difficult to measure from observations. In Fig. 3 we plot the abundance predictions of the

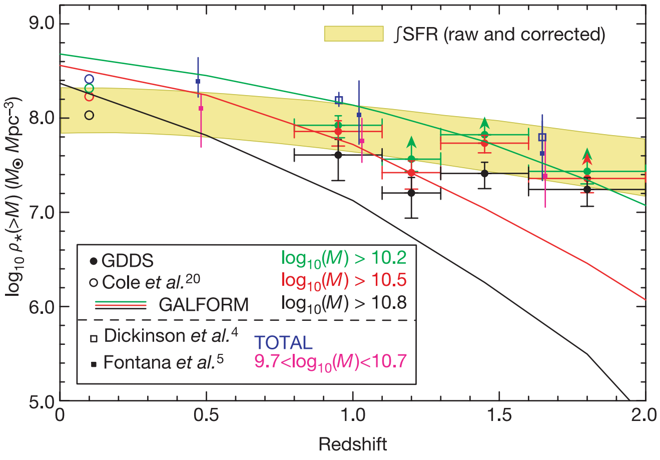

Figure 3 Mass density in stars versus redshift. Values from our spectroscopic sample are compared with previous estimates which are all based on photometric redshifts[4,5] (except for the local $z = 0.1$ point[20]). We plot the cumulative mass density of galaxies (converted to our IMF choice; error bars are 1σ) more massive than a given mass threshold (see key for threshold colour coding). Theoretical 'GALFORM' models are also plotted (see text). The shaded region shows the result of integrating the Universal UV-derived star-formation history with and without a dust extinction correction.

'GALFORM' models[14,22] which satisfy the first two constraints. It is evident in this model that massive galaxies disappear much more rapidly than we see in our data; this is because the model stellar mass build-up traces the merging of cold dark matter haloes. In particular, GALFORM has a strong dependence of evolutionary rate on mass which is not seen in our data. A similar theoretical comparison was made on the Hubble Deep South photometric data with similar conclusions[5].

We note that our measured abundance of massive galaxies at $z \approx 2$ does not violate the boundary constraints of cold dark matter models, by which we mean taking the predicted abundance of $z = 2$ massive dark matter haloes[23] and scaling by the cosmological baryon / dark matter density[2] ($\Omega_b/\Omega_m = 0.17$). This gives a predicted baryonic mass density of $\sim 10^8 M_\odot\ \mathrm{Mpc}^{-3}$ in haloes with baryonic masses $> 10^{11} M_\odot$, a factor of ten above our measurements. Thus the models can match our densities if only ~10% of the baryons in massive haloes are converted to stars by $z = 2$. However, we note that in the Universe today, the stellar density[20] $\Omega_\star = 0.004$ gives $\Omega_\star/\Omega_b = 0.1$; this would imply that massive haloes at $z = 2$ have managed to convert baryons into stars with the same overall efficiency as the average Universe had achieved by $z = 0$. Massive haloes must have much greater star-formation efficiencies at earlier times.

Models have been proposed[13,24] which adjust the star-formation histories in this way, and which would be more in accord with our findings of a high abundance of massive galaxies at early times. However, they fail to match existing data on galaxy colours[25,26] or the galaxy luminosity function[13], so we defer detailed comparison to future work.

What is observationally clear is that we have measured directly the abundance of massive galaxies out to $z = 2$ for the first time from a highly complete, deep and relatively wide area survey with secure redshifts and spectroscopic classifications for galaxies. We find (with 99% confidence) that at least two-thirds of the mass in these objects has formed since $z = 1.8$. However, we do not find a more rapid evolution of the giant population compared to the Universal average, as would be expected if stellar mass grew simply proportionally to dark matter assembly. At $z \lesssim 2$ we find that much of the mass is in galaxies with old stellar populations; these objects are plausible precursors of modern massive elliptical galaxies. This is broadly consistent with developing ideas that models of galaxy formation have to be tuned towards earlier star-formation in high-mass haloes. The abundance of massive galaxies at $z \lesssim 2$ is now firmly established, and will provide the vital missing leg in the tripod of key observations required to understand how galaxies form. ☐

Table 1 **Stellar mass density measurements in the Universe**

$\log M_{\mathrm{lim}}$	BG03 IMF				Kennicutt IMF			
	z range	$\log \rho$	$\log \rho_{\mathrm{lo}}$	$\log \rho_{\mathrm{hi}}$	$\log \rho$	$\log \rho_{\mathrm{lo}}$	$\log \rho_{\mathrm{hi}}$	Complete?
10.2	0.8–1.1	7.92	7.79	8.02	7.82	7.67	7.92	Y
10.2	1.1–1.3	7.56	7.43	7.66	7.47	7.34	7.58	N
10.2	1.3–1.6	7.82	7.73	7.90	7.71	7.62	7.79	N
10.2	1.6–2.0	7.43	7.30	7.54	7.34	7.21	7.44	N
10.5	0.8–1.1	7.86	7.70	7.97	7.72	7.54	7.84	Y
10.5	1.1–1.3	7.42	7.25	7.55	7.34	7.17	7.47	Y
10.5	1.3–1.6	7.73	7.63	7.82	7.62	7.51	7.71	Y
10.5	1.6–2.0	7.36	7.21	7.47	7.26	7.11	7.37	N
10.8	0.8–1.1	7.61	7.34	7.77	7.46	7.13	7.64	Y
10.8	1.1–1.3	7.21	6.94	7.37	6.92	6.49	7.14	Y
10.8	1.3–1.6	7.41	7.25	7.53	7.24	7.04	7.38	Y
10.8	1.6–2.0	7.24	7.06	7.37	6.96	6.74	7.11	Y

Measurements are shown as a function of galaxy mass threshold and redshift. ρ is the stellar mass density in galaxies with stellar masses $>M_{\mathrm{lim}}$ in $M_\odot\ \mathrm{Mpc}^{-3}$. The values of ρ_{hi} and ρ_{lo} are the 1σ upper and lower limits from counting statistics. BG03 IMF mass thresholds and mass densities can be multiplied by 1.82 to convert to the Salpeter IMF.

Methods

Stellar mass fitting

We adopt a cosmology[2] of $\Omega_m = 0.3$, $\Omega_\Lambda = 0.7$, $H_0 = 70\ \mathrm{km\,s^{-1}\,Mpc^{-1}}$ and use Vega magnitudes. For the mass-function analysis, we use GDDS galaxies with $K < 20.6$ and $0.8 < z < 2$ (150 galaxies; 89% spectroscopic completeness based on ref. 17 identification confidence classes ≥ 2; galaxies without spectroscopic redshifts are assigned to their photometric redshifts). To account for the higher priority given to red galaxies in the slit-mask design we use the 'sampling weights' from ref. 17, which are the selection probabilities for spectroscopy as a function of $I - K$ and K.

For each galaxy we derive the most likely stellar mass and a range of uncertainty. These are derived by evaluating against model optical-IR SEDs to determine the M/L_K ratio, and hence the mass. We note that a variety of approaches to accomplish this have been described in the literature which vary in the level of detail in which they treat star formation. For example, ref. 20 used a simple set of monotonic star-formation histories (SFH) with a varying e-folding timescale and a fixed dust law. A potential problem is posed by the fact that real galaxies have more complex SFHs; for example, a recent star-burst can make an old galaxy temporarily bluer and lead to an underestimate of M/L using this method. One approach to account for this effect is to introduce a second young SED component[5] superimposed on the old population; this can be computationally expensive depending on the amount of freedom allowed for the second component.

In a spectroscopic sample there is no degeneracy between SED model fitting and photometric redshift (which is also based on SED fitting). We adopt two-component modelling (using PEGASE.2[21] to calculate spectra) in order to be able to assess the possible biases due to starbursts on the calculated masses, and allow a range of dust extinction ($0 \leq A_V \leq 2$ mag) and metallicity ($0.0004 \leq Z \leq 0.02$). The primary component is modelled using a star-formation rate SFR $\propto \exp(-t/\tau)$ with $\tau = 0.1, 0.2, 0.5, 1, 2, 4, 8$ and 500 Gyr (the first approximates an instantaneous starburst and the last a constant SFR). The secondary component is a starburst, modelled with a $\tau = 0.1$ Gyr exponential, which can occur at any time and have a mass between 10^{-4} and twice that of the primary component. The model age is constrained to be less than that of the Universe at the appropriate redshift, but any formation epoch is allowed. Like all studies of high redshift star-formation, we must assume a universal initial mass function (IMF). We primarily use the BG03 IMF[27] which fits local cosmic luminosity densities well; it has a similar high-mass slope to the classical Salpeter IMF[28] but with a more realistic break at $0.5 M_\odot$. Stars with masses below the break never contribute significantly to optical/IR light, so the overall effect is to re-scale the total stellar masses to more reasonable values. Similarly we re-scale literature Salpeter based numbers[4,5,20] to the BG03 IMF using $M_{\mathrm{SP}} = 1.82 M_{\mathrm{BG}}$. Our results are robust for any reasonable choice of IMF with a similar slope; to illustrate this, we have also calculated masses using the popular Kennicutt IMF[29].

Our approach is to find via exhaustive grid search all models consistent with the $VIz'K$ photometry in the observed frame of each galaxy. This colour set is available for all galaxies, and covers rest-frame UV through near IR. We do not include the actual spectra (apart from the redshift information) in the fits because of variable quality and signal-to-noise ratio, but we find the spectral classes are broadly consistent with the best photometric SED fits. The full distribution function of allowed masses were calculated by Monte Carlo re-sampling of the photometric errors. The final masses and error bars represent the mean and standard deviation of this full distribution function. Typically, we find the masses are fitted to ±0.17 dex in the $K < 20.6$ sample. The stellar masses are very robust against the details of the fitting. Using the Monte Carlo machinery to investigate the effect of different assumptions about metallicity, dust and bursts, we find that the largest effect is due to bursts. If we disallowed bursts, then the masses typically decrease by only 0.2 dex. Finally, we note that the variation in M/L_K over the range $1 < z < 2$ is constrained by the age of the Universe (6–3 Gyr); typically the maximum range in our sample is a factor of three.

Received 4 January; accepted 24 May 2004; doi:10.1038/nature02667.

1. Blumenthal, G. R., Faber, S. M., Primack, J. R. & Rees, M. J. Formation of galaxies and large-scale structure with cold dark matter. *Nature* **311,** 517–525 (1984).
2. Spergel, D. N. *et al.* First-year Wilkinson Microwave Anisotropy Probe (WMAP) observations: Determination of cosmological parameters. *Astrophys. J. Suppl.* **148,** 175–194 (2003).
3. Brinchmann, J. & Ellis, R. S. The mass assembly and star formation characteristics of field galaxies of known morphology. *Astrophys. J.* **536,** L77–L80 (2000).
4. Dickinson, M., Papovich, C., Ferguson, H. C. & Budavári, T. The evolution of the global stellar mass density at $0 < z < 3$. *Astrophys. J.* **587,** 25–40 (2003).
5. Fontana, A. *et al.* The assembly of massive galaxies from near-infrared observations of the Hubble Deep Field-South. *Astrophys. J.* **594,** L9–L12 (2003).
6. Drory, N. *et al.* The Munich Near-Infrared Cluster Survey: Number density evolution of massive field galaxies to $z \sim 1.2$ as derived from the K-band-selected survey. *Astrophys. J.* **562,** L111–L114 (2001).
7. Franx, M. *et al.* A significant population of red, near-infrared-selected high-redshift galaxies. *Astrophys. J.* **587,** L79–L82 (2003).
8. Madau, P. *et al.* High-redshift galaxies in the Hubble Deep Field: colour selection and star formation history to $z \sim 4$. *Mon. Not. R. Astron. Soc.* **283,** 1388–1404 (1996).
9. Steidel, C. C., Adelberger, K. L., Giavalisco, M., Dickinson, M. & Pettini, M. Lyman-break galaxies at $z \sim 4$ and the evolution of the ultraviolet luminosity density at high redshift. *Astrophys. J.* **519,** 1–17 (1999).
10. Lotz, J. M., Ferguson, H. C. & Bohlin, R. C. Mid-ultraviolet determination of elliptical galaxy abundances and ages. *Astrophys. J.* **532,** 830–844 (2000).
11. Vogt, N. P. *et al.* Optical rotation curves of distant field galaxies: Sub-L* systems. *Astrophys. J* **479,** L121–L124 (1997).
12. Gebhardt, K. *et al.* The DEEP Groth strip Survey. IX. Evolution of the fundamental plane of field galaxies. *Astrophys. J.* **597,** 239–262 (2003).
13. Kauffmann, G., Colberg, J. M., Diaferio, A. & White, S. D. M. Clustering of galaxies in a hierarchical universe - II. Evolution to high redshift. *Mon. Not. R. Astron. Soc.* **307,** 529–536 (1999).

14. Baugh, C. M., Benson, A. J., Cole, S., Frenk, C. S. & Lacey, C. in *The Mass of Galaxies at Low and High Redshift* (eds Bender, R. & Renzini, A.) 91–96 (ESO Astrophysics Symposia, Berlin, Springer, 2003).
15. Rix, H. & Rieke, M. J. Tracing the stellar mass in M51. *Astrophys. J.* **418,** 123–134 (1993).
16. Bell, E. F., McIntosh, D. H., Katz, N. & Weinberg, M. D. The optical and near-infrared properties of galaxies. I. Luminosity and stellar mass functions. *Astrophys. J. Suppl.* **149,** 289–312 (2003).
17. Abraham, R. G. *et al.* The Gemini Deep Deep Survey: I. Introduction to the survey, catalogs and composite spectra. *Astron. J.* **127,** 2455–2483 (2004).
18. Savaglio, S. *et al.* The Gemini Deep Deep Survey. II. Metals in star-forming galaxies at redshift $1.3 < z < 2$. *Astrophys. J.* **602,** 51–65 (2004).
19. Schmidt, M. Space distribution and luminosity functions of quasi-stellar radio sources. *Astrophys. J.* **151,** 393–409 (1968).
20. Cole, S. *et al.* The 2dF galaxy redshift survey: near-infrared galaxy luminosity functions. *Mon. Not. R. Astron. Soc.* **326,** 255–273 (2001).
21. Fioc, F. & Rocca-Volmerange, B. PEGASE: a UV to NIR spectral evolution model of galaxies. Application to the calibration of bright galaxy counts. *Astron. Astrophys.* **326,** 950–962 (1997).
22. Granato, G. L. *et al.* The infrared side of galaxy formation. I. The local universe in the semianalytical framework. *Astrophys. J.* **542,** 710–730 (2000).
23. Sheth, R. K. & Tormen, G. Large-scale bias and the peak background split. *Mon. Not. R. Astron. Soc.* **308,** 119–126 (1999).
24. Somerville, R. S., Primack, J. R. & Faber, S. M. The nature of high-redshift galaxies. *Mon. Not. R. Astron. Soc.* **320,** 504–528 (2001).
25. Somerville, R. S. *et al.* The redshift distribution of near-infrared-selected galaxies in the Great Observatories Origins Deep Survey as a test of galaxy formation scenarios. *Astrophys. J.* **600,** L135–L138 (2004).
26. Stanford, S. A. *et al.* The evolution of early-type field galaxies selected from a NICMOS map of the Hubble Deep Field North. *Astron. J.* **127,** 131–155 (2004).
27. Baldry, I. K. & Glazebrook, K. Constraints on a universal stellar initial mass function from ultraviolet to near-infrared galaxy luminosity densities. *Astrophys. J.* **593,** 258–271 (2003).
28. Salpeter, E. E. The luminosity function and stellar evolution. *Astrophys. J.* **121,** 161–167 (1955).
29. Kennicutt, R. C. The rate of star formation in normal disk galaxies. *Astrophys. J.* **272,** 54–67 (1983).
30. Coleman, G. D., Wu, C.-C. & Weedman, D. W. Colors and magnitudes predicted for high redshift galaxies. *Astrophys. J. Suppl.* **43** (Suppl.), 393–416 (1980).

Acknowledgements This work is based on observations obtained at the Gemini Observatory, which is operated by AURA under a co-operative agreement with the NSF on behalf of the Gemini partnership: NSF (US), PPARC (UK), NRC (Canada), CONICYT (Chile), ARC (Australia), CNPq (Brazil) and CONICET (Argentina); it is also based on observations made at the Las Campanas Observatory of the Carnegie Institution of Washington. K.G. and S.S. acknowledge funding from the David and Lucille Packard Foundation; S.S. is on leave of absence from the Osservatorio Astronomica di Roma, Italy. R.A. acknowledges funding from NSERC and from the Government of Ontario through a Premier's Research Excellence award. H.-W.C. acknowledges support by NASA through a Hubble Fellowship grant from the Space Telescope Science Institute, which is operated by the Association of Universities for Research in Astronomy, Inc., under NASA contract.

Competing interests statement The authors declare that they have no competing financial interests.

Correspondence and requests for materials should be addressed to K.G. (kgb@pha.jhu.edu).

* * *

Old galaxies in the young Universe

A. Cimatti[1], E. Daddi[2], A. Renzini[2], P. Cassata[3], E. Vanzella[3], L. Pozzetti[4], S. Cristiani[5], A. Fontana[6], G. Rodighiero[3], M. Mignoli[4] & G. Zamorani[4]

[1]*INAF - Osservatorio Astrofisico di Arcetri, Largo E. Fermi 5, I-50125, Firenze, Italy*
[2]*European Southern Observatory, Karl-Schwarzschild-Strasse 2, D-85748, Garching, Germany*
[3]*Dipartimento di Astronomia, Università di Padova, Vicolo dell'Osservatorio, 2, I-35122 Padova, Italy*
[4]*INAF - Osservatorio Astronomico di Bologna, via Ranzani 1, I-40127, Bologna, Italy*
[5]*INAF - Osservatorio Astronomico di Trieste, via Tiepolo 11, I-34131 Trieste, Italy*
[6]*INAF - Osservatorio Astronomico di Roma, via dell'Osservatorio 2, Monteporzio, Italy*

More than half of all stars in the local Universe are found in massive spheroidal galaxies[1], which are characterized by old stellar populations[2,3] with little or no current star formation. In present models, such galaxies appear rather late in the history of the Universe as the culmination of a hierarchical merging process, in which larger galaxies are assembled through mergers of smaller precursor galaxies. But observations have not yet established how, or even when, the massive spheroidals formed[2,3], nor if their seemingly sudden appearance when the Universe was about half its present age (at redshift $z \approx 1$) results from a real evolutionary effect (such as a peak of mergers) or from the observational difficulty of identifying them at earlier epochs. Here we report the spectroscopic and morphological identification of four old, fully assembled, massive (10^{11} solar masses) spheroidal galaxies at $1.6 < z < 1.9$, the most distant such objects currently known. The existence of such systems when the Universe was only about one-quarter of its present age shows that the build-up of massive early-type galaxies was much faster in the early Universe than has been expected from theoretical simulations[4].

In the ΛCDM scenario[5], galaxies are thought to build up their present-day mass through a continuous assembly driven by the hierarchical merging of dark matter haloes, with the most massive galaxies being the last to form. However, the formation and evolution of massive spheroidal early-type galaxies is still an open question.

Recent results indicate that early-type galaxies are found up to

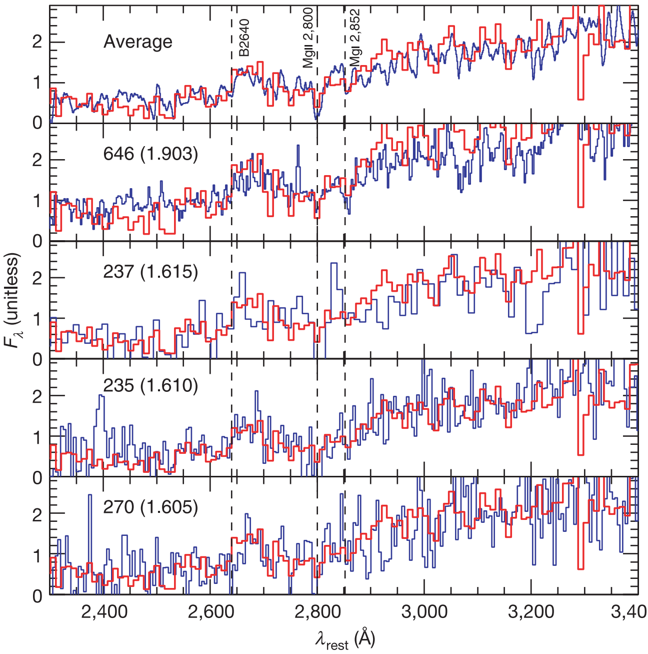

Figure 1 The individual and average spectra of the detected galaxies. From bottom to top: the individual spectra smoothed to a 16 Å boxcar (26 Å for ID 237) and the average spectrum of the four old galaxies ($z_{\text{average}} = 1.68$). The red line is the spectrum of the old galaxy LBDS 53w091 ($z = 1.55$) used to search for spectra with a similar continuum shape. Weak features in individual spectra (for example, MgII 2,800 Å and the 2,640 Å continuum break, B2640) become clearly visible in the average spectrum. The object ID 235 has also a weak [OII] 3,727 Å emission (not shown here). The spectra were obtained with ESO VLT + FORS2, grisms 200I ($R(1'') \approx 400$) (ID 237) and 300I ($R(1'') \approx 600$) (IDs 235, 270, 646), 1.0″ wide slit and $\lesssim 1''$ seeing conditions. The integrations times were 3 hours for ID 237, 7.8 hours for IDs 235 and 270, and 15.8 hours for ID 646. For ID 646, the ESO/GOODS public spectrum was co-added to our K20 spectrum (see Supplementary Table 1). 'Dithering' of the targets along the slits was applied to remove efficiently the CCD fringing pattern and the strong OH sky lines in the red. The data reduction was done with the IRAF software package[16]. The spectrophotometric calibration of all spectra was achieved and verified by observing several standard stars. The average spectrum, corresponding to 34.4 hours integration time, was obtained by co-adding the individual spectra convolved to the same resolution, scaled to the same arbitrary flux (that is, with each spectrum having the same weight in the co-addition), and assigning wavelength-dependent weights which take into account the noise in the individual spectra due to the OH emission sky lines.